Nuclear Physics B179 (1981) 33–48

KAON-NUCLEON PARAMETERS

A.D. MARTIN

Department of Physics, University of Durham, England

Received 13 May 1980
(Final version received 25 August 1980)

A multichannel analysis of low-energy $\bar{K}N$ data is presented, which simultaneously is required to satisfy dispersion relation constraints coming partly from the measured real parts of the forward $K^{\pm}N$ amplitudes and partly from forward $K^-p \to \bar{K}^0 n$ and $K_L^0 p \to K_S^0 p$ data. The $K^{\pm}N$ scattering lengths are determined, and the KN nucleon coupling constants found to be $g_\Lambda^2 = 13.9 \pm 2.6$ and $g_\Sigma^2 \leqslant 3.3 \pm 1.1$. The forward amplitudes are tabulated.

1. Introduction

The problems associated with the determination of the low-energy $\bar{K}N$ amplitudes and coupling constants are longstanding. On their own, the available low-energy data on K^-p and $(K_L^0 p)$ initiated reactions are insufficient for a unique multichannel $(\bar{K}N, \pi\Sigma, \pi\Lambda)$ analysis. We might at least expect the $\bar{K}N \to \bar{K}N$ amplitudes to be well determined. However, due to the presence of the $\Lambda(1405)$ resonance just below the K^-p threshold, the determination is far from precise enough to be able to extrapolate the amplitudes reliably into this (unphysical) region.

A significant source of independent information has come, via forward dispersion relations, from the detailed Coulomb-nuclear interference measurements [1, 2] of the real parts of the forward KN amplitudes. Apart from the Λ and Σ couplings, the primary unknown in the evaluation of the forward dispersion relations is the unphysical region contribution. In practice the contribution is calculated by extrapolation of the $\bar{K}N$ amplitudes corresponding to a K-matrix parametrization of the low-energy K^-p scattering data. Now the K-matrix solutions are far from unique*. It is therefore clear that, with the new forward data, the dispersion relations can "pass judgement" on the various parametrizations. They were all found to fail in the sense that the "output" value of the real part of the K^-p amplitude at threshold obtained from the dispersion relation is very different to the "input" value given by the K-matrix parametrization used to evaluate the low-energy dispersion integrals**. This is not surprising because the evaluation of the dispersion integral

* A good illustration of this ambiguity is given in ref. [3].
** Examples of this mismatch can be found in ref. [1].

over the $\Lambda(1405)$ resonance depends sensitively on the energy dependence prescribed for the $\bar{K}N$ amplitude. On the other hand it does mean that imposing "input-output" consistency will be a valuable constraint on a low-energy $\bar{K}N$ parametrization.

To impose this constraint, a simultaneous analysis of the low-energy K^-p (and $K^0_L p$) reaction data and of the dispersion relation information was performed [4]. It was found impossible to obtain a satisfactory overall fit using energy-independent K (or $M \equiv K^{-1}$) matrices. It was necessary to introduce extra parameters in the $I = 0$ M-matrix. An effective range form was used. This contrasts with the constant M-matrix analyses without analyticity constraints, where the low-energy $\bar{K}N$ data can be well described, and moreover where the solution was not unique. An interesting feature of the parametrization [4] obtained imposing analyticity constraints is that the real part of the $I = 1$ $\bar{K}N$ scattering length is increased from 0 to 0.35 fm. As a consequence, the description of the low-energy $K^-p \to \bar{K}^0 n$ is systematically above the data.

At that time the real part data were better for $K^\pm p$, than for $K^\pm n$, dispersion relations. Subsequently $K^0_L p \to K^0_S p$ data have become available in the 0.5 – 1.2 GeV/c region [5], and also much higher precision $K^-p \to \bar{K}^0 n$ forward scattering data in the 0.5 – 1 GeV/c interval [6]. These data give information on $|D^+_n - D^-_n|$ and $|D^-_p - D^-_n|$ respectively, where $D^\pm_N$ are the real parts of the $K^\pm N$ forward amplitudes. They therefore tighten the dispersion relation constraints, particularly those for $K^\pm n$. Here we present a determination of the $\bar{K}N$ parameters taking the new data into account. Moreover, we give a realistic estimation of the errors, and study the effect of including a $\Sigma(1385)$ contribution in the dispersion relations. We also consider the information so far available from the TST experiment [7] on low-energy K^-p interactions. The wide range of constraints imposed on, and the self-consistency of, the dispersion relations mean that we can give definitive values of the couplings, the subtraction parameters and the real parts of the forward $K^\pm N$ amplitudes.

2. Kaon-nucleon forward dispersion relations

In order to make use of the experimental information available for the real parts of the forward amplitudes we use the once subtracted dispersion relations

$$D^-_N(\omega) = D_N(0) + \sum_Y \frac{\omega R_Y g^2(YK^-N)}{\omega_Y(\omega_Y - \omega)} + \frac{\omega}{\pi} P \int_{\omega_{th}}^{\infty} \left[\frac{A^-_N(\omega')}{\omega' - \omega} - \frac{A^+_N(\omega')}{\omega' + \omega} \right] \frac{d\omega'}{\omega'}, \qquad (1)$$

with $N = n, p$, where $F^\pm_N = D^\pm_N + iA^\pm_N$ are the forward $K^\pm N$ scattering amplitudes in the laboratory frame, normalized so that the optical theorem is

$$A^\pm_N = \frac{k_L}{4\pi} \sigma_T(K^\pm N), \qquad (2)$$

and where ω and k_L are the kaon energy and momentum in the laboratory frame.

The summation is over the Λ and Σ pole terms, and

$$R_Y = [(m_Y - m_p)^2 - m_K^2]/4m_p^2 .$$

We shall use g_Y^2 to denote $g^2(YK^-p)$. Only isospin $I = 1$ $\bar{K}N$ contributions enter the $K^\pm n$ relations; in this case $g^2(\Sigma K^- n) = 2g_\Sigma^2$.

We evaluate the dispersion relations at those values of ω for which information exists for $D^-(\omega)$, and at values of $-\omega$ for which $D^+(\omega) = D^-(-\omega)$ is known. We use the Coulomb interference measurements [1, 2] of $D_N^\pm$, together with the information from the charge exchange [6, 8] and regeneration [5] processes. We may express the differential cross section for forward scattering for the latter processes in terms of $K^\pm N$ amplitudes. In the laboratory frame we obtain

$$\frac{d\sigma}{d\Omega_L}(K^-p \to \bar{K}^0 n) = |D_p^- - D_n^-|^2 + |A_p^- - A_n^-|^2 \tag{3}$$

$$4\frac{d\sigma}{d\Omega_L}(K_L^0 p \to K_S^0 p) = |D_n^+ - D_n^-|^2 + |A_n^+ - A_n^-|^2 . \tag{4}$$

Thus the use of charge exchange data at a given energy, ω, requires the evaluation of both the $K^\pm p$ and the $K^\pm n$ relations at ω, whereas the regeneration data require the $K^+ n$ relation to be evaluated at ω and $-\omega$.

The dispersion integrals over A^- from ω_{th} to $k_L = 0.23$ GeV/c are calculated using the S-wave $\bar{K}N$ M-matrix parametrization. We consider the inclusion of a $\Sigma(1385)$ contribution in sect. 5. The integrals over A^- from 0.23 to 200 GeV/c and over A^+ from threshold to 200 GeV/c are determined using smooth interpolations of the measured $K^\pm p$ and $K^\pm n$ total cross sections. Actually in the region $0.36 < k_L < 1.3$ GeV/c* we use $\sigma_T(K^- n)$ as calculated from the LBL $\bar{K}N$ partial-wave analysis [9]. This shows some small but significant departures from the values extracted from the observed $\sigma_T(K^- d)$ data, which are crucial to include if the high precision LBL $K^- p \to \bar{K}^0 n$ forward data [6] are to be used as constraints. Finally the small contributions from $k_L = 200$ GeV/c to infinity are calculated assuming $(A^- - A^+) \sim \omega^{0.45}$ and $(A^- + A^+) \sim \omega^{1.06}$.

3. Combined M-matrix and dispersion relation analysis

As explained in sect. 1, the $K^+ p$ and $K^\pm n$ forward dispersion relations provide a unique type of constraint on a low-energy $\bar{K}N$ parametrization. The value of the self-consistency requirement is enhanced by the proximity of the $\Lambda(1405)$, which gives a sizeable contribution to the dispersion integrals.

The procedure is to perform an M-matrix analysis of the low-energy $\bar{K}N$ data, simultaneously using these same parameters to evaluate the low-energy dispersion integrals over A^-, and requiring that the $K^+ p$ and $K^\pm n$ relations are satisfied at all

* In the small interval below 0.36 GeV/c we estimate $\sigma_T(K^- n)$ as in ref. [4].

energies at which reliable information on the real parts, $D^{\pm}$, exists. To be precise, we vary the S-wave M-matrix parameters and the four dispersion relations parameters [$D_p(0)$, $D_n(0)$, g_Λ^2 and g_Σ^2 of eqs. (1)] to obtain an optimum fit to

(a) the low energy K^-p and K_L^0p data and at-rest branching ratios,
(b) the measured values of $D_p^{\pm}$ and D_n^- below 3 GeV/c,
(c) the self-consistency of the $\bar{K}N$ amplitudes at threshold,
(d) the known KN scattering lengths,
(e) the forward $K^-p \to \bar{K}^0n$ differential cross-section data,
(f) the forward $K_L^0p \to K_S^0p$ differential cross-section data.

We discuss the selection of data used in the fit in sect. 4. There we also show the quality of the description of the low-energy K^-p initiated data, and of the forward charge exchange and regeneration data.

To achieve a satisfactory fit it was necessary to introduce extra parameters in the $I = 0$ M-matrix. We use an effective range form $\underset{\sim}{M} = \underset{\sim}{A} + \underset{\sim}{R}k^2$, where k is the c.m. K^-p momentum, and a constant $I = 1$ M-matrix. Corrections are included for electromagnetic mass differences and for Coulomb effects in the K^-p channel in the usual way [10].

TABLE 1

The parameter values for the combined M-matrix and dispersion relation analysis of kaon-nucleon data

Subtraction and coupling constants	
$D_p(0) = -2.83 \pm 0.40$ fm	$D_n(0) = -0.64 \pm 0.16$ fm
$g_\Lambda^2 = 13.9 \pm 2.6$	$g_\Sigma^2 = 3.3 \pm 1.1$
$I = 0$ M-matrix parameters: $\underset{\sim}{M} = \underset{\sim}{A} + \underset{\sim}{R}k^2$	
$\underset{\sim}{A}$ (fm^{-1})	$\underset{\sim}{R}$ (fm)
$A_{KK} = -0.07^{+0.56}_{-0.10}$	$R_{KK} = 0.18^{+0.56}_{-0.32}$
$A_{K\Sigma} = -1.02^{+0.23}_{-0.74}$	$R_{K\Sigma} = 0.20 \pm 1.1$
$A_{\Sigma\Sigma} = 1.94^{+1.13}_{-0.78}$	$R_{\Sigma\Sigma} = 1.11^{+2.8}_{-1.7}$
$I = 1$ $K \equiv M^{-1}$ matrix elements in fm	
$K_{KK} = 1.06^{+0.38}_{-0.29}$	$K_{K\Sigma} = -1.32^{+1.2}_{-0.8}$
$K_{K\Lambda} = -0.29^{+3.6}_{-1.2}$	$K_{\Sigma\Sigma} = 0.27^{+3.5}_{-3.1}$
$K_{\Sigma\Lambda} = 1.54^{+3.8}_{-0.9}$	$K_{\Lambda\Lambda} = -1.02^{+3.3}_{-2.6}$

The errors quoted for a parameter are calculated by fixing that parameter at certain selected values and re-minimizing with respect to the remaining parameters.

The parameter values of the optimum fit to the combined data are listed in table 1. The value of g_Σ^2 is an upper bound since it includes both Σ and $\Sigma(1385)$ contributions. The effect of explicitly including the $\Sigma(1385)$ is discussed in sect. 5.

A careful error analysis was undertaken; the errors given in table 1 are the appropriate MINOS errors of the CERN Minuit programme. We see the dispersion relation parameters are reasonably well determined, whereas this is not the case for the M-matrix elements. The lack of uniqueness of the M-matrix parameters is not surprising since we have no data for the $\pi Y \to \pi Y$ channels, $Y = \Sigma$ or Λ. Nevertheless, the simultaneous requirements of the data and the dispersion relations do severely constrain the elastic $\bar{K}N \to \bar{K}N$ amplitudes, T_{KK}. Consequently the complex

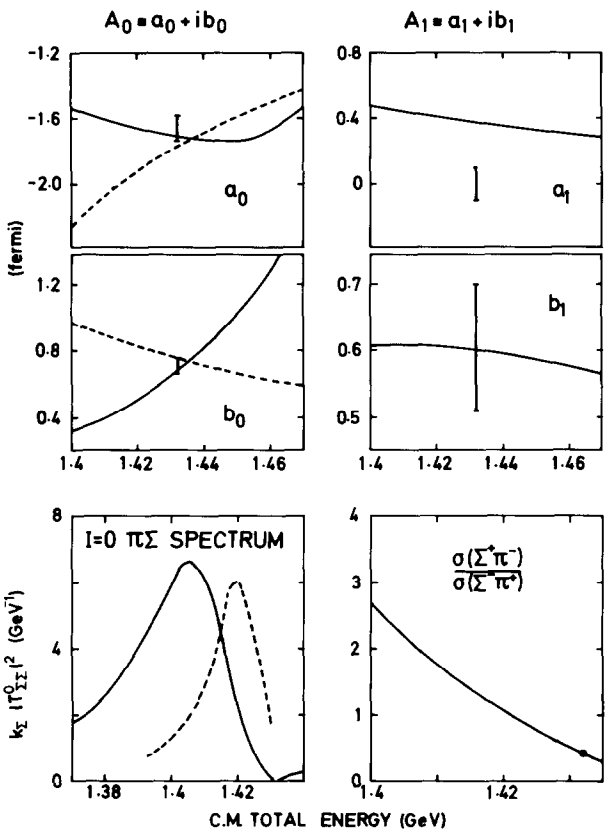

Fig. 1. The continuous curves show the energy dependence of the $\bar{K}N$ scattering lengths, $A_I = a_I + ib_I$, corresponding to the parameters of table 1. The error bars give the range of the threshold values of A_I found in the K-matrix analyses without analyticity constraints. The use of a Breit–Wigner parametrization for the $I = 0$ S-wave (see sect. 5) leads to the dashed curves and does not give a satisfactory description of the data. We also show the S-wave contribution to the $I = 0$ $\pi\Sigma$ spectrum and the ratio of Σ^+/Σ^- production below threshold.

"scattering lengths", A_I, are well determined, where A_I are defined such that

$$T^I_{KK} = \frac{A_I}{1 - ikA_I}. \tag{5}$$

They are displayed as a function of energy in fig. 1. In particular, note that $A_0 \equiv a_0 + ib_0$ has the characteristic energy dependence shown by the continuous curve. This behaviour is an encouraging indication of the reliability of the analyticity constraints for two reasons. First the $I = 0$ amplitude extrapolates to give an acceptable $\Lambda(1405)$ resonance, with a "sheet 2" pole at $E_R = 1411 - i\ 15$ MeV and a $\pi\Sigma$ mass spectrum as shown in fig. 1. This is a far from trivial result. Secondly the $I = 0$ S-wave determined in the LBL partial-wave analysis [9] corresponds to $A_0 = 1.0 + i\ 2.7$ fm at 360 MeV/c, which supports the rapidly increasing b_0 of fig. 1.

The values of the scattering lengths at the K^-p threshold are

$$\begin{aligned} A_0 &= -1.70 + i\ 0.68 \text{ fm}, \\ A_1 &= 0.37 + i\ 0.60 \text{ fm}. \end{aligned} \tag{6}$$

The preliminary measurements of the energy shift and width of the 2P→ 1S X-ray transition in kaonic atoms of hydrogen have been interpreted in terms of an extremely small K^-p scattering length [11]. We find it impossible to achieve a combined fit with the additional constraint of the small K^-p scattering length implied by these mesonic atom results.

The real parts of the forward amplitudes resulting from the $K^\pm p$ and $K^\pm n$ dispersion relations are shown in figs. 2 and 3. As they are frequently used in

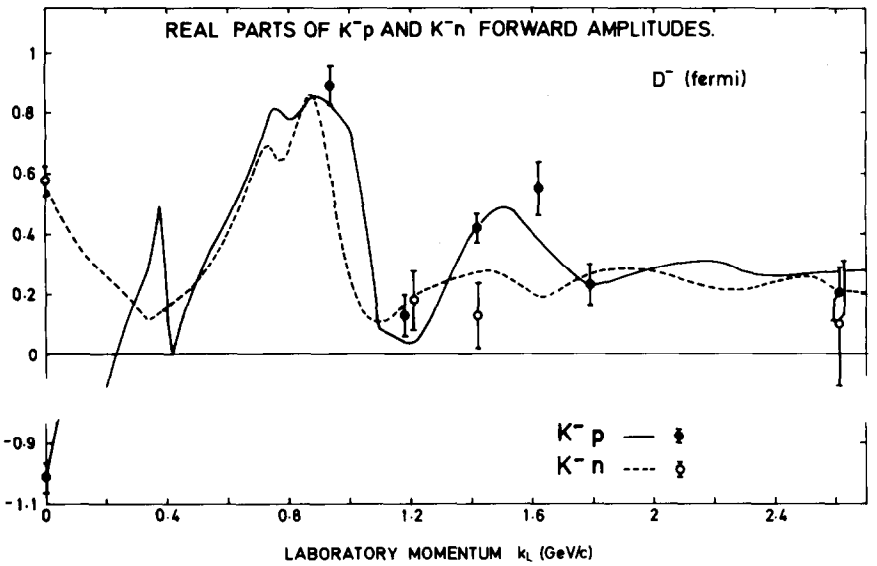

Fig. 2. The curves are the real parts of the K^-p and K^-n forward amplitudes found in the combined dispersion relation and M-matrix analysis. The data are from refs. [1, 2].

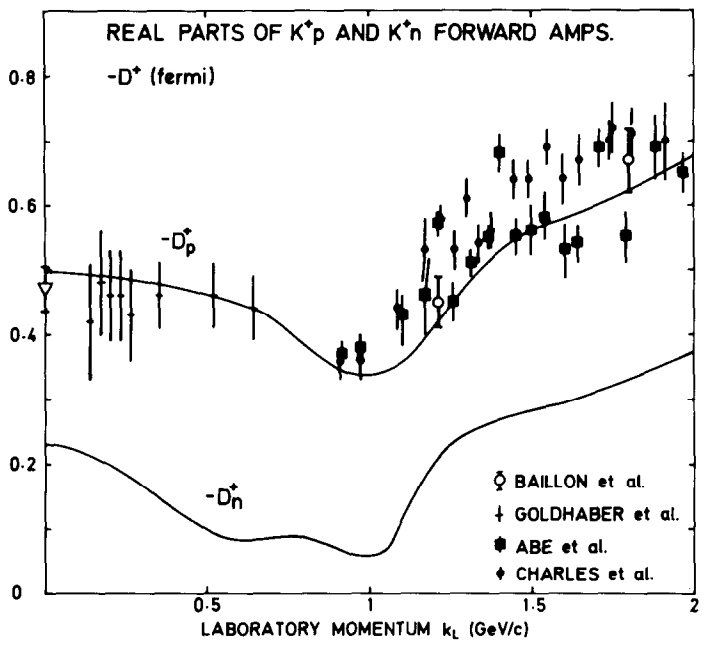

Fig. 3. The curves are the real parts of the K^+p and K^+n forward amplitudes found in the analysis. Note that the real parts are negative. Only the open data points are used in the analysis, the remaining ones are obtained by extrapolating the K^+p elastic differential cross section data to 0° and are taken from the compilation of ref. [12].

partial-wave analyses, we list selected values in table 2. For K^+p, we compare our predictions with real parts obtained by extrapolating [12] the K^+p elastic differential cross section data [13] to 0°:

$$\frac{d\sigma}{d\Omega_L} = |D_p^+|^2 + |A_p^+|^2 . \tag{7}$$

We do not use this information in the fit, since K^+p is adequately constrained by the threshold value and by the Coulomb-interference measurements. For the other charge configurations $|D|/|A|$ is too small for the elastic data to be useful.

It is instructive to present the dispersion relation results in terms of the "discrepancy functions", $\Delta(\omega)$, introduced by the CERN-Caen group [1]. Their procedure* was to rewrite the $K^\pm p$ relation of eq. (1) in the form

$$[D_p^-(\omega) - I(\omega)](\omega - \bar{\omega}_Y) = (\omega - \bar{\omega}_Y)D_p(0) + \frac{R_\Lambda G^2}{\bar{\omega}_Y}\omega , \tag{8}$$

where $I(\omega)$ denotes the contribution of the integral term of eq. (1), and where the Λ

* Note that in ref. [1] $\Delta(\omega)$ is defined in terms of D^+, and not D^-. Therefore, to compare fig. 4 with ref. [1] we must reflect about $\omega = 0$.

TABLE 2

The real parts of the forward $K^{\pm}N$ amplitudes (fm) resulting from the combined dispersion relation and M-matrix analysis

k_L (GeV/c)	$D(K^-p)$	$D(K^-n)$	$D(K^+p)$	$D(K^+n)$
0.0	−0.98	0.54	−0.50	−0.23
0.35	0.36	0.12	−0.48	−0.14
0.375	0.50	0.15	−0.48	−0.13
0.4	0.16	0.17	−0.48	−0.13
0.425	0.03	0.18	−0.47	−0.12
0.5	0.26	0.25	−0.46	−0.10
0.6	0.46	0.40	−0.45	−0.08
0.7	0.69	0.67	−0.43	−0.09
0.75	0.82	0.68	−0.41	−0.09
0.8	0.79	0.69	−0.38	−0.09
0.85	0.82	0.84	−0.36	−0.08
0.9	0.86	0.81	−0.35	−0.07
0.95	0.82	0.53	−0.34	−0.06
1.0	0.74	0.25	−0.34	−0.06
1.05	0.44	0.15	−0.34	−0.07
1.1	0.09	0.11	−0.35	−0.12
1.2	0.05	0.19	−0.42	−0.21
1.3	0.20	0.24	−0.48	−0.26
1.4	0.41	0.28	−0.52	−0.27
1.5	0.50	0.27	−0.56	−0.28
1.6	0.41	0.21	−0.58	−0.30
1.8	0.24	0.27	−0.62	−0.33
2.0	0.29	0.28	−0.67	−0.38
2.2	0.31	0.23	−0.72	−0.41
2.4	0.27	0.25	−0.76	−0.44
2.6	0.28	0.22	−0.81	−0.47

and Σ poles are approximated by an effective pole at $\tilde{\omega}_Y$ with a coupling $G^2 = g_\Lambda^2 + 0.84 g_\Sigma^2$. They called the left-hand side of eq. (8) a "discrepancy function", and denoted it by $\Delta_p(\omega)$. $\Delta_p(\omega)$ is known at those values of ω at which $D^-(\omega)$ is measured. By comparing $\Delta_p(\omega)$ to a linear form in ω, the values of G^2 and $D_p(0)$ were determined*.

We show our results in terms of $\Delta(\omega)$ in fig. 4. We stress that our analysis uses eq. (1) directly, and not the approximate form, eq. (8). Near the pole positions we do not have a linear form for $\Delta_p(\omega)$. Moreover, the lines are not simply the best fits to the data points shown; there are other constraints. For example, in the case of the $K^{\pm}n$ relation, the forward $K^-p \to \bar{K}^0 n$ data constrain D_n^- and the regeneration data constrain $|D_n^+ - D_n^-|$.

* Although G^2 is not sensitive to the precise choice of $\tilde{\omega}_Y$, the same is not true for $D_p(0)$. To determine $D_p(0)$ we need to know both g_Λ^2 and g_Σ^2 and so have to evaluate both $K^{\pm}p$ and $K^{\pm}n$ relations.

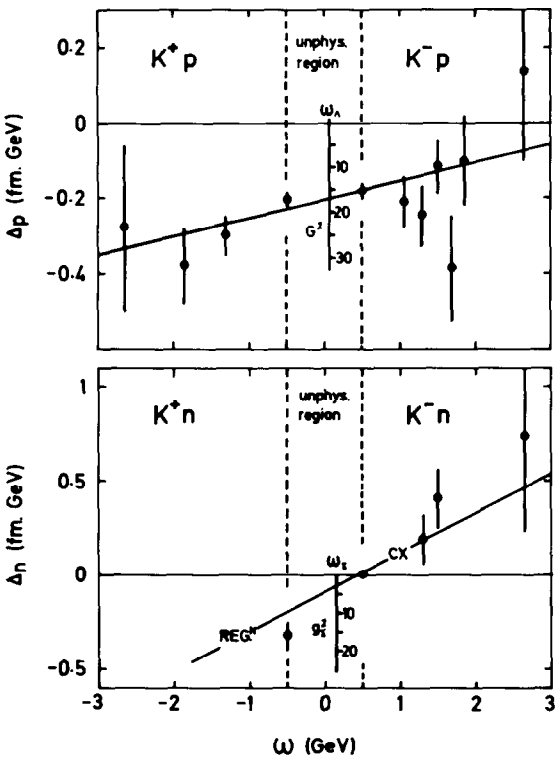

Fig. 4. Plots of Δ_p and Δ_n versus ω obtained from the $K^{\pm}p$ and $K^{\pm}n$ dispersion relation results of eq. (1). $\Delta(\omega)$ is defined by eq. (8). The symbols REG^N and CX are to indicate the extra constraints coming from regeneration and charge exchange data.

4. Description of experimental data

The combined analysis fits to a wide range of data and it is important to give appropriate weight to the various data sets. The real part information that is closest to the low-energy region is of most value in constraining the kaon-nucleon parameters. Also we note that the low-energy dispersion integrals have to be calculated for many different values of ω at *each* iteration of the M-matrix parameters. For these reasons we do not attempt to fit to all the available data.

The low-energy K^-p data [14, 15] are shown in fig. 5. In the fit of sect. 3 we used representative data at 110 and 240 MeV/c, together with the following values of the observed K^-p at-rest branching ratios,

$$(\Sigma^+\pi^- + \Sigma^-\pi^+)/Y\pi = 0.664 \pm 0.011\,[16],$$

$$\Sigma^-\pi^+/\Sigma^+\pi^- = 2.36 \pm 0.04\,[16],$$

$$\Lambda\pi^0/(\Lambda\pi^0 + \Sigma^0\pi^0) = 0.189 \pm 0.015\,[14],$$

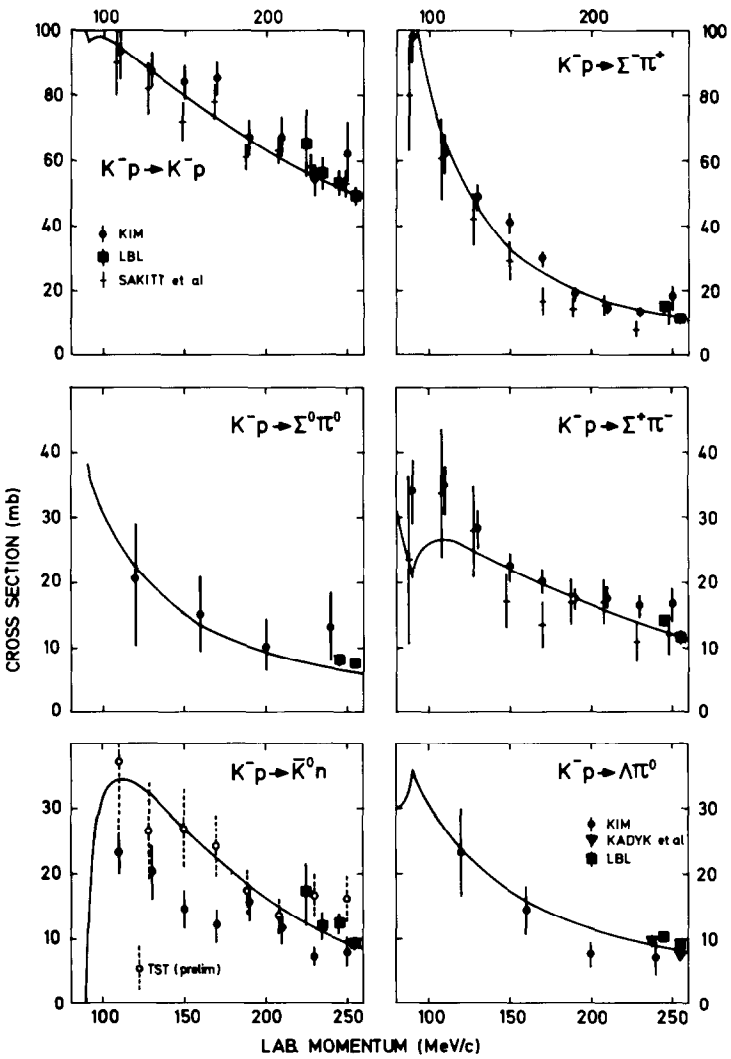

Fig. 5. The low-energy K^-p data from refs. [14, 15, 7, 17]. The curves are calculated from the M-matrix parameters of table 1.

and representative $K^0_L p$ data [17] at 1455 MeV. The curves on fig. 5 correspond to the M-matrix solution of table 1.

The TST collaboration [7] have data on the low-energy K^-p channels. They plan to provide statistics comparable to, or better than Kim [14], but with a more careful study of the possible sources of bias than hitherto. So far at-rest branching ratios are available [16], but only preliminary results for the scattering data. In the preliminary data (see, Bedford, ref. [7]) the most significant departure from the data of Kim [14] is for $K^-p \to \bar{K}^0 n$, see fig. 5. The confirmation of this result is important because such a

change was predicted in the original M-matrix analysis with analyticity constraints [4]. In the present analysis we take the $K^-p \to \bar{K}^0 n$ cross section to be 33 ± 4 mb at 110 MeV/c and 12 ± 1.5 mb at 240 MeV/c.

Consider now the forward $K^-p \to \bar{K}^0 n$ data to be used to determine $|D_p^- - D_n^-|$, via eq. (3). The analysis of ref. [4] imposed constraints arising from the observed dips in the data [8] at 0.3 and 1.3 GeV/c. We also use these data. Recently the LBL group have made high precision counter measurements of $K^-p \to \bar{K}^0 n$ in the $0.5 - 1$ GeV/c momentum range [6]. The results for the forward cross section are shown in fig. 6. To use such accurate data to constrain $|D_p^- - D_n^-|$ requires care. Over much of the energy range the second term, $|A_p^- - A_n^-|^2$, of eq. (3) dominates the forward cross section and so the results depend sensitively on the values used for the K^-p and K^-n total cross sections. It is therefore important to use $\sigma_T(K^-n)$ as determined by the LBL partial-wave analysis [9] of this and other high precision data. The dashed line in fig. 6. shows the contribution of the "total cross section" term, $|A_p^- - A_n^-|^2$, to forward $K^-p \to \bar{K}^0 n$. We conclude that it is only in the region 0.9–0.96 GeV/c that the new data should be used to limit $|D_p^- - D_n^-|$. Inspection of the rapid energy dependence inherent in $D_p^- - D_n^-$ in this small momentum interval show the value of the constraint. The final prediction, including the contribution of the dispersion relation real part, is shown by the continuous curve on fig. 6. The residual disagreement between the curve and the data below 0.9 GeV/c can be accounted for by small changes in either the K^-n or the K^-p total cross section. For example, if we

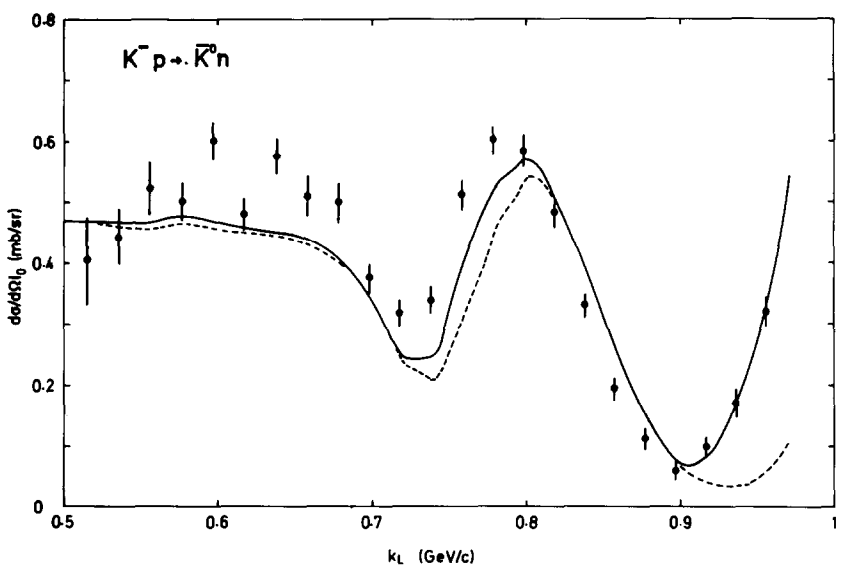

Fig. 6. The charge exchange differential cross section at 0°. The data are from ref. [6]. The dashed curve is the prediction using only the imaginary part of the forward amplitude as given by the K^-p and K^-n total cross sections. The continuous curve is the result of including the real part as given by the $K^{\pm}p$ and $K^{\pm}n$ dispersion relations.

keep the K^-p total cross section fixed, then the $K^-p \to \bar{K}^0 n$ forward data indicate that the K^-n total cross section should be decreased by about 1 mb in the region of 0.6 GeV/c and increased by about 1 mb near 0.85 GeV/c from the values calculated from the analysis of ref. [9]. We do not make these total cross section adjustments since the only effect of such changes is a slight shift of the dispersion relation prediction for D_n^- near 0.7 GeV/c.

Recently the regeneration process $K_L^0 p \to K_S^0 p$ has been measured in the 0.5–1.2 GeV/c region by three independent groups [5]. The values of the forward cross section are displayed in fig. 7. These data are particularly useful as the regeneration amplitude is proportional to the difference of the $K^{\pm}n$ amplitudes, see eq. (4). Again the contribution of the total cross section term, $|A_n^+ - A_n^-|^2$, is shown by the dashed curve, and indicates that the data in the region 0.6–0.8 GeV/c will give a good measurement of $|D_n^+ - D_n^-|$. We fit to representative data in this interval. The final description, including the real part contribution, is shown by the continuous curve on fig. 7.

The importance of the regeneration data is that they act as a constraint on D_n^+ in a region where no other experimental information exists. Previous evaluations of the $K^{\pm}n$ relation relied on fitting to the K^+n threshold value. The value is obtained from the "known" K^+N scattering lengths and, for example, taken to be $D_n^+(m_K) = -0.23 \pm 0.03$ and -0.21 ± 0.07 fm in refs. [18] and [4] respectively. For instance ref. [4] uses

$$\alpha_0 = 0.04 \pm 0.10 \text{ fm}, \qquad \alpha_1 = -0.32 \pm 0.02 \text{ fm}$$

for isospin 0 and 1 scattering lengths. The latter value is well established by K^+p data, but α_0 is extracted from K^+d data. Recently the uncertainties in this determination have been emphasized, and a value of $\alpha_0 = -0.23 \pm 0.18$ fm proposed [19]. Clearly the errors on the "input" value of $D_n^+(m_K)$ have been underestimated, particularly in ref. [18]. In the present analysis we fitted to $D_n^+(m_K)$ calculated from the new value of α_0. However, the "output" values of $D_{p,n}^+$ correspond to

$$\alpha_0 = 0.02 \text{ fm}, \qquad \alpha_1 = -0.33 \text{ fm}.$$

5. The $\Sigma(1385)$ and $\Lambda(1405)$ contributions

By comparing table 1 with the results of ref. [4], we see that the dispersion relation parameters are stable to the introduction of the new data into the analysis. The MINOS errors of table 1 are more realistic than those of ref. [4] which represent the diagonal errors of the error matrix and do not take correlations into account. It is interesting to note that g_Σ^2 is better determined than g_Λ^2. However, in the parametrization of sect. 3 the $\Sigma(1385)$ was omitted.

If a $\Sigma(1385)$ pole term is included, the optimum fit to the data has a resonance coupling compatible with zero, but it is hard to separate the Σ and the small $\Sigma(1385)$

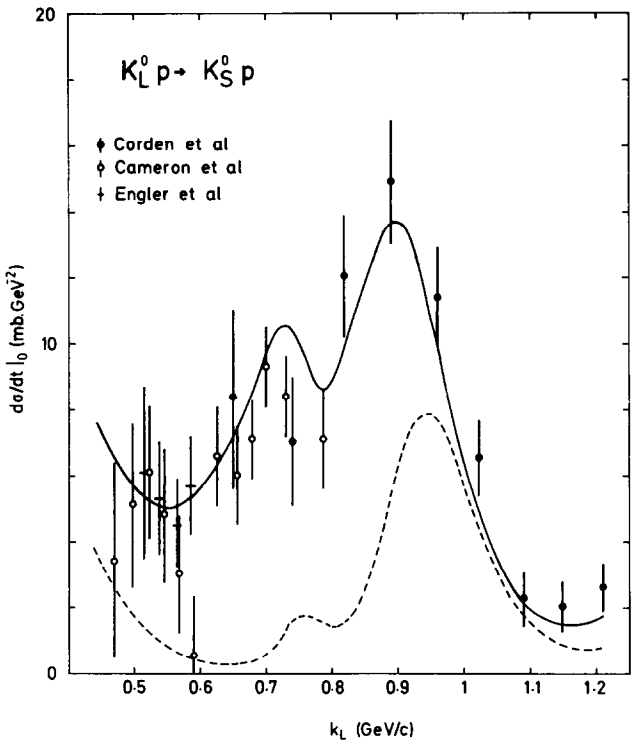

Fig. 7. The regeneration differential cross section, $d\sigma/dt$, at $t = 0$. The data are from refs. [5]. The dashed curve is the prediction using only the imaginary part of the forward amplitude as given by the $K^{\pm}n$ total cross sections. The continuous curve is the result of including the real part from the $K^{\pm}n$ dispersion relations.

contributions. To examine the effect of the $\Sigma(1385)$ we repeated the analysis including the $\Sigma(1385)$ in the dispersion relations with a coupling estimated from SU(3). To be explicit we included, in eq. (1) for D_p^-, a term

$$\frac{\omega k_R^2 G^2}{m_p^2(\omega_R - \omega)\omega_R},$$

where k_R and ω_R are the K^-p c.m. momentum and laboratory energy at the pole position, and where the coupling $G^2(\Sigma(1385)K^-p) = 3.5$ is taken from ref. [20]. The pole occurs with twice the strength in the $K^{\pm}n$ relation. In this case the dispersion relation parameters corresponding to the best fit are

$$g_\Lambda^2 = 14.1\,, \qquad g_\Sigma^2 = 0.04\,,$$

$$D_p(0) = -2.71\ \text{fm}\,, \qquad D_n(0) = -0.32\ \text{fm}\,.$$

We do not list the M-matrix parameters, but note that the scattering lengths at the K^-p threshold are

$$A_0 = -1.62 + i\,0.71 \text{ fm}, \qquad A_1 = 0.53 + i\,0.60 \text{ fm}.$$

However, the fit is not satisfactory; χ^2 per degree of freedom has increased from 0.9 to 1.4. The data prefer a smaller $\Sigma(1385)$ contribution. The effect of fixing the $\Sigma(1385)$ contribution decreases the K^-N real parts by about 0.03 fm in the 1–3 GeV/c range.

Turning now to the $\Lambda(1405)$, we have already remarked that the $K^{\pm}p$ dispersion relation constraints have led to M-matrix parameters which extrapolate to a $\Sigma\pi$ spectrum in good agreement with the $\Lambda(1405)$ peak observed in production experiments. We gave the $\Lambda(1405)$ parameters in sect. 3. In the above parametrization the $\Lambda(1405)$ arises as a $\bar{K}N$ "bound-state" resonance, whereas in the quark model we expect a CDD pole interpretation [21]. In the latter approach the simplest parametrization is a Breit–Wigner description of the $\Lambda(1405)$. All the $I = 0$ K-matrix elements (and also A_0) would then have a pole

$$K_{ij} = \frac{g_i g_j}{E_0 - E},$$

but, unfortunately, considerably displaced from 1405 MeV. If the $I = 0$ S-wave is parametrized in terms of g_1, g_2 and E_0, such that the amplitude has a pole near 1405 MeV, then no adequate description of the data is possible. Indeed, the parametrization leads to an energy dependence of A_0 shown by the dashed curves on fig. 1, which are very different to those required by the data.

To be fair, no adequate fit was possible with a three parameter $I = 0$ constant M-matrix either; effective range parameters are necessary. Thus we are led to include a background contribution

$$K_{ij} = \frac{g_i g_j}{E_0 - E} + (K_0)_{ij}.$$

Unfortunately, in such a fit the pole residues become very small and K_0 is such that we revert to the $\bar{K}N$ "bound-state" description. McGinley [22] reaches a similar conclusion. He also performs model calculations of the $\Lambda(1405)$ and finds, for example, that, if the CDD pole is broad enough, the resulting K-matrix may have no nearby pole.

The dynamical origin of the $\Lambda(1405)$ remains an open question, which must await $\Sigma\pi \to \Sigma\pi$ data. With the advent of high-energy hyperon beams, such information is accessible, namely to study π exchange reactions of the type $\Sigma N \to \Sigma\pi N$ with the produced $\Sigma\pi$ system going forward.

6. Conclusion

With the exception of the preliminary kaonic hydrogen atom results [11], it is possible to obtain a self-consistent M-matrix description of all the low-energy $\bar{K}N$

data, simultaneously satisfying the $K^{\pm}p$ and $K^{\pm}n$ dispersion relation constraints coming partly from the measured real parts of the forward $K^{\pm}N$ amplitudes and partly from the forward $K^-p \to \bar{K}^0 n$ and $K^0_L p \to K^0_S p$ data.

The dispersion relations are stable to the introduction of the recent data. Indeed the wide range of input information means definitive predictions can now be obtained from these relations. The coupling constants are found to be

$$g^2_\Lambda = 13.9 \pm 2.6\,, \qquad g^2_\Sigma = 3.3 \pm 1.1\,,$$

where the latter value is an upper bound as it represents the sum of the Σ and $\Sigma(1385)$ contributions; however, the data prefer a small $\Sigma(1385)$ coupling. The K^+N scattering lengths resulting from the relations are

$$\alpha_0 = 0.02\,\text{fm}\,, \qquad \alpha_1 = -0.33\,\text{fm}\,,$$

and those for K^-N are

$$A_0 = -1.70 + i\,0.68\,\text{fm}\,,$$

$$A_1 = 0.37 + i\,0.60\,\text{fm}\,.$$

The real parts of the forward $K^{\pm}p$ and $K^{\pm}n$ amplitudes are tabulated up to 2.6 GeV/c. We emphasize that, because of the interlocking constraints, these values are more reliable than those calculated using either $K^{\pm}p$ or $K^{\pm}n$ relations on their own.

The absence of $\pi Y \to \pi Y$ information means the M-matrix parameters are far from unique. However the low-energy data on the $\bar{K}N$ initiated channels together with the KN analyticity constraints means that the $\bar{K}N \to \bar{K}N$ amplitudes are well determined. Indeed, support for imposing analyticity constraints comes from the preliminary TST data [7] for $K^-p \to \bar{K}^0 n$ below 250 MeV/c. The new measurements are found to disagree with the early data as was anticipated, and required, by the original analysis with analyticity constraints (ref. [4]).

The data and the constraints lead to the characteristic energy dependence of A_0 shown in fig. 1. The corresponding $I = 0$ $\bar{K}N$ amplitude, on the one hand extrapolates to predict a $\Lambda(1405)$ in agreement with $\Sigma\pi$ production, and on the other, is compatible with the S-wave found in the $\Lambda(1520)$ region. The dynamical nature of the $\Lambda(1405)$ is not revealed.

References

[1] P. Baillon et al., Nucl. Phys. B105 (1976) 365
[2] P. Jenni et al., Nucl. Phys. B105 (1976) 1;
P. Baillon et al., Phys. Lett. 50B (1974) 377;
P. Baillon et al., Nucl. Phys. B107 (1976) 189
[3] Y.A. Chao et al., Nucl. Phys. B56 (1973) 46
[4] A.D. Martin, Phys. Lett. 65B (1976) 346

[5] W. Cameron et al., Nucl. Phys. B132 (1978) 189;
A. Engler et al., Phys. Rev. D18 (1978) 3061;
M.J. Corden et al., Nucl. Phys. B155 (1979) 13
[6] M. Alston-Garnjost et al., Phys. Rev. D17 (1978) 2226
[7] R. Nowak et al., Nucl. Phys. B139 (1978) 61;
N.H. Bedford, Durham University thesis (1979);
D.J. Miller, Proc. Workshop on Kaon-nucleon physics, Rome (1980) to be published
[8] R.D. Tripp, Proc. Oxford Conf. on Baryon resonances (1976) p. 496
[9] M. Alston-Garnjost et al., Phys. Rev. D18 (1978) 183
[10] R.H. Dalitz and S.F. Tuan, Ann. of Phys. 10 (1960) 307
[11] J.D. Davies et al., Phys. Lett. 83B (1979) 55;
C.J. Batty, Proc. Workshop on Kaon-nucleon physics, Rome (1980) to be published
[12] N.M. Queen, Univ. of Birmingham Report UB-KP-1-78 (1978)
[13] G. Goldhaber et al., Phys. Rev. Lett. 9 (1962) 135;
K. Abe et al., Phys. Rev. D11 (1975) 1719;
B.J. Charles et al., Nucl. Phys. B131 (1977) 7
[14] W.E. Humphrey and R.R. Ross, Phys. Rev. 127 (1962) 1305;
M. Sakitt et al., Phys. Rev. 139B (1965) 719;
J.K. Kim, Columbia University report, Nevis 149 (1966)
[15] T.S. Mast et al., Phys. Rev. D11 (1975) 3078; D14 (1976) 13;
R.D. Tripp, private communication
[16] D. Tovee et al., Nucl. Phys. B33 (1971) 493;
R. Nowak et al., Nucl. Phys. B139 (1978) 61
[17] J.A. Kadyk et al., Phys. Rev. Lett. 17 (1966) 599; UCRL 18325 (1968);
G.A. Sayer et al., Phys. Rev. 169 (1968) 1045
[18] P. Baillon et al., Phys. Lett. 61B (1976) 171
[19] B.R. Martin, J. Phys. G4 (1978) 335
[20] M.M. Nagels et al., Nucl. Phys. B147 (1979) 189
[21] R.H. Dalitz, HR-70-03, presented at Duke University Hyperon Conf. (1970)
[22] J.G. McGinley, Oxford University thesis (1979)